Dual functions for OVAAL in initiation of RAF/MEK/ERK prosurvival signals and evasion of p27-mediated cellular senescence

Ben Sang[a,1], Yuan Yuan Zhang[b,c,1], Su Tang Guo[d,e], Ling Fei Kong[b], Qiong Cheng[b], Guang Zhi Liu[b], Rick F. Thorne[b,f], Xu Dong Zhang[b,g], Lei Jin[c,2], and Mian Wu[a,b,2]

[a]Division of Molecular Medicine, Hefei National Laboratory for Physical Sciences at Microscale, the Chinese Academy of Sciences (CAS) Key Laboratory of Innate Immunity and Chronic Disease, CAS Center for Excellence in Cell and Molecular Biology, School of Life Sciences, University of Science and Technology of China, Hefei 230026, China; [b]Translational Research Institute, Henan Provincial People's Hospital, Academy of Medical Science, Zhengzhou University, 450003 Zhengzhou, China; [c]School of Medicine and Public Health, The University of Newcastle, Callaghan, NSW 2308, Australia; [d]Department of Molecular Biology, Shanxi Cancer Hospital and Institute, 030013 Taiyuan, Shanxi, China; [e]Department of Pathology, Shanxi Cancer Hospital and Institute, 030013 Taiyuan, Shanxi, China; [f]School of Environmental and Life Sciences, The University of Newcastle, Callaghan, NSW 2308, Australia; and [g]School of Biomedical Sciences and Pharmacy, The University of Newcastle, Callaghan, NSW 2308, Australia

Edited by Michael G. Rosenfeld, University of California, San Diego, La Jolla, CA, and approved October 29, 2018 (received for review April 5, 2018)

Long noncoding RNAs (lncRNAs) function through a diverse array of mechanisms that are not presently fully understood. Here, we sought to find lncRNAs differentially regulated in cancer cells resistant to either TNF-related apoptosis-inducing ligand (TRAIL) or the Mcl-1 inhibitor UMI-77, agents that act through the extrinsic and intrinsic apoptotic pathways, respectively. This work identified a commonly up-regulated lncRNA, ovarian adenocarcinoma-amplified lncRNA (OVAAL), that conferred apoptotic resistance in multiple cancer types. Analysis of clinical samples revealed OVAAL expression was significantly increased in colorectal cancers and melanoma in comparison to the corresponding normal tissues. Functional investigations showed that OVAAL depletion significantly inhibited cancer cell proliferation and retarded tumor xenograft growth. Mechanically, OVAAL physically interacted with serine/threonine-protein kinase 3 (STK3), which, in turn, enhanced the binding between STK3 and Raf-1. The ternary complex OVAAL/STK3/Raf-1 enhanced the activation of the RAF protooncogene serine/threonine-protein kinase (RAF)/mitogen-activated protein kinase kinase 1 (MEK)/ERK signaling cascade, thus promoting c-Myc–mediated cell proliferation and Mcl-1–mediated cell survival. On the other hand, depletion of OVAAL triggered cellular senescence through polypyrimidine tract-binding protein 1 (PTBP1)–mediated p27 expression, which was regulated by competitive binding between OVAAL and p27 mRNA to PTBP1. Additionally, c-Myc was demonstrated to drive OVAAL transcription, indicating a positive feedback loop between c-Myc and OVAAL in controlling tumor growth. Taken together, these results reveal that OVAAL contributes to the survival of cancer cells through dual mechanisms controlling RAF/MEK/ERK signaling and p27-mediated cell senescence.

OVAAL | c-Myc | p27 | proliferation | senescence

Assessment of the human genome shows that genes encoding long noncoding RNAs (lncRNAs) are more abundant than protein-coding genes. The lncRNAs are a structurally and functionally diverse class of RNAs, although they are generally classified as transcripts >200 nt in length with no protein-coding potential (1, 2). Notably, some lncRNAs also bear cryptic ORFs, and there are examples where these ORFs have been shown to be translated to small peptides (3, 4). Functionally, lncRNAs play a crucial role in the regulation of numerous biological processes, such as proliferation, survival, migration, and senescence, along with genomic stability (2, 5–10). Mechanistically, lncRNAs regulate diverse cellular processes through interaction with other cellular molecules, including DNA, RNA, and protein (11–13). Moreover, the peptides encoded by lncRNAs can also serve as functional entities, and, in some rare examples, lncRNAs have been shown to have functions as both RNA and protein, so-called bifunctional lncRNAs.

It is increasingly evident that aberrations within the noncoding genome drive important cancer phenotypes (2) and that these alterations can be associated with prognosis, efficacy of treatment, and patient survival (14–16). Resisting cell apoptosis and sustaining proliferative signaling are two hallmarks of cancer that limit the efficacy of cancer treatment (17). Indeed, numerous lncRNAs affect pathogenesis of cancer by regulating cell apoptosis and proliferation (8, 12, 18). For instance, the lncRNA gene SAMMSON, whose expression was detectable in more than 90% of human melanomas, promotes melanoma growth and survival (15, 19). Moreover, lncRNA MEG3 is down-regulated in prostate cancer tissues in comparison to adjacent normal tissues and inhibits the intrinsic cell survival pathway via reducing the expression levels of Bcl-2, enhancing Bax protein expression, and activating caspase-3 (20). Overexpression of the lncRNA PVT1 also promotes ovarian cancer cell resistance to cisplatin by

Significance

Here, we report that the long noncoding RNA (lncRNA) ovarian adenocarcinoma-amplified lncRNA (OVAAL) is a mediator of cancer cell resistance, counteracting the effects of apoptosis-inducing agents acting through both the extrinsic and intrinsic pathways. Building upon previous reports associating OVAAL amplification with ovarian and endometrial cancers, we now show that OVAAL overexpression occurs during the pathogenesis of colorectal cancer and melanoma. Mechanistically, our findings also establish that OVAAL expression more generally contributes a prosurvival role to cancer cells under steady-state conditions. OVAAL accomplishes these actions utilizing distinct functional modalities: one promoting activation of RAF/MEK/ERK signaling and the other blocking cell entry into senescence. Our study demonstrates that expression of a single OVAAL in cancer cells drives two distinct but coordinated actions contributing to cancer pathology.

Author contributions: B.S., X.D.Z., L.J., and M.W. designed research; B.S., Y.Y.Z., and S.T.G. performed research; G.Z.L. contributed new reagents/analytic tools; Y.Y.Z., L.F.K., Q.C., R.F.T., and L.J. analyzed data; and R.F.T., X.D.Z., L.J., and M.W. wrote the paper.

The authors declare no conflict of interest.

This article is a PNAS Direct Submission.

[1]B.S. and Y.Y.Z. contributed equally to this work.

[2]To whom correspondence may be addressed. Email: lei.jin@newcastle.edu.au or wumian@ustc.edu.cn.

This article contains supporting information online at www.pnas.org/lookup/suppl/doi:10.1073/pnas.1805950115/-/DCSupplemental.

Published online November 26, 2018.

inhibiting apoptotic pathways (21). Similarly, certain lncRNAs have been shown to counteract the entry of cells into senescence, thought to be a failsafe mechanism acting to prevent cell transformation (22). For instance, lncRNA FAL-1 was found to be increased in ovarian cancer and shown to repress p21-induced senescence (10). Nevertheless, knowledge of the functional roles played by lncRNAs in controlling cell apoptosis, proliferation, and senescence in cancer remains poorly understood.

One of the known drivers that limits tumor progression via apoptosis, serine/threonine-protein kinase 3 (STK3; also known as MST2), is an STK activated by the stress-induced apoptotic pathway that limits tumor progression via apoptosis (23). Moreover, STK3 is known to form an inhibitory complex with Raf-1, but when dissociated from Raf-1, it can bind to tumor suppressor protein RASSF1A, resulting in the induction of apoptosis (23, 24). Conversely, phosphorylation of Raf-1 at serine 259 by Akt inhibits Raf-1 activity, whereas serine/threonine protein phosphatases 1 and 2a (PP1 and PP2A) dephosphorylate Raf-1 at serine 259, thus preventing Raf-1 protein degradation (25). STK3 promotes Raf-1 activation via phosphatase PP2A-mediated dephosphorylation of Raf-1 at Ser259, thus activating RAF protooncogene serine/threonine-protein kinase (RAF)/mitogen-activated protein kinase kinase 1 (MEK)/ERK signaling and consequently promoting cell survival and proliferation (26). Of additional relevance to this report, polypyrimidine tract-binding protein 1 (PTBP1) is aberrantly overexpressed and promotes cell proliferation in various types of cancer (27, 28). PTBP1 is an RNA-binding protein that exerts effects on RNA processing, including specifically enhancing the translation of p27 (27–29), notably regarded as a key effector of cellular senescence (30).

Here, we demonstrate that a c-Myc–regulating ovarian adenocarcinoma-amplified lncRNA (OVAAL) plays dual roles in both promoting cell proliferation and escaping apoptosis and senescence. We identified OVAAL in a screen designed to identify lncRNAs involved in conferring resistance to both intrinsic and extrinsic apoptotic pathways. Mechanistically, OVAAL binds to STK3 and subsequently facilitates the association between STK3 and Raf-1, leading to activation of RAF/MEK/ERK cascade. The activated RAF/MEK/ERK pathway promotes cell proliferation and survival via preventing proteasome-mediated degradation of c-Myc and Mcl-1, respectively (31, 32). Moreover, OVAAL also binds to PTBP1 and reduces the recruitment of PTBP1 to the internal ribosome entry site (IRES) of p27 mRNA, thus imparting an inhibitory effect on p27 mRNA translation and preventing cells from diverting to cellular senescence (29, 30, 33). Collectively, our study shows that OVAAL is essential for cell survival, proliferation, and evasion from cellular senescence, implicating potential benefits of targeting OVAAL in the treatment of cancer.

Results

Screening of lncRNAs Involved in Cancer Cell Evasion of Extrinsic and Intrinsic Apoptotic Pathways Identifies OVAAL. To identify functional lncRNA(s) responsible for cancer cells evading apoptosis, we generated ME4405 TNF-related apoptosis-inducing ligand (TRAIL)–selected (TRAIL.S) and ME4405 UMI-77–selected (UMI-77.S) cell sublines that were resistant to TRAIL and the Mcl-1 inhibitor UMI-77, respectively, after long-term exposure to drug treatment (Fig. 1*A* and *SI Appendix*, Fig. S1*A*). ME4405 melanoma cells were chosen because they are relatively sensitive to both TRAIL and UMI-77 among a panel of melanoma cell lines (*SI Appendix*, Fig. S1*B*). TRAIL treatment serves to activate the extrinsic apoptotic pathway, whereas UMI-77 targets Mcl-1, a key antiapoptotic Bcl-2 family protein that serves to restrain the intrinsic apoptotic pathway. By performing RNA-sequencing analysis, we found 37 up-regulated lncRNAs in common between TRAIL.S and UMI-77.S cells (Fig. 1*B* and *SI Appendix*, Table S1), suggesting these lncRNAs may function in both extrinsic and intrinsic apoptotic pathways. Among the top five up-regulated lncRNA candidates (OVAAL, PHKA2-AS1, LOC105372218, LOC105370413, and LINC00221), as confirmed by qPCR (*SI Appendix*, Fig. S1*C*), only knockdown of OVAAL (34, 35) significantly overcame resistance to TRAIL and UMI-77 (*SI Appendix*, Fig. S1 *D* and *E*).

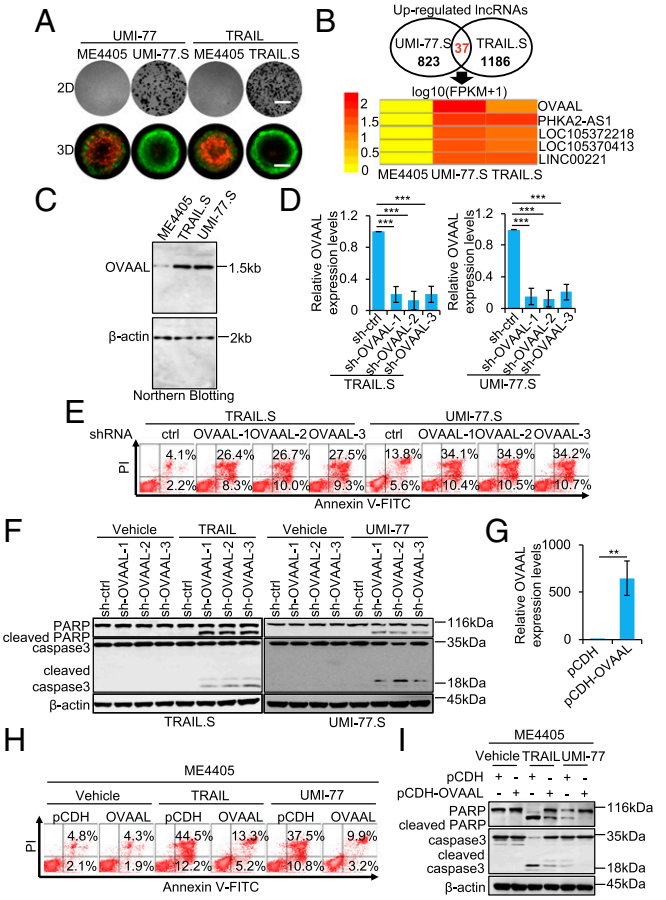

Fig. 1. OVAAL is selectively up-regulated and confers resistance against cancer cells to TRAIL and the Mcl-1 inhibitor UMI-77. (*A*) ME4405 TRAIL.S and ME4405 UMI-77.S cell sublines display resistance to TRAIL (25 ng/mL) and the Mcl-1 inhibitor UMI-77 (4 μM) as shown in colony formation assays (2D) and hanging drop assays (3D) ($n = 3$). (Scale bars: 2D, 1 cm; 3D, 25 μm.) (*B*) Thirty-seven lncRNAs were up-regulated in common between selected cells in comparison to ME4405 cells. The heat map illustrates the five most up-regulated lncRNAs. (*C*) OVAAL was up-regulated in TRAIL.S and UMI-77.S cells as shown in Northern blotting. β-Actin mRNA was used as a loading control ($n = 3$). Depletion of OVAAL in resistant TRAIL.S and UMI-77.S cells using three independent shRNA targeting vectors (*D*) results in increased apoptosis as measured by annexin V-FITC staining in cells treated with vehicle control (ctrl), TRAIL, or UMI-77 for 24 h (*E*) and accompanying activation of caspase-3 and cleavage of PARP visualized by Western blotting (*F*) ($n = 3$; mean ± SD; Student's *t* test). OVAAL overexpression in parental ME4405 cells (*G*) treated with vehicle ctrl, TRAIL (25 ng/mL), or UMI-77 (4 μM) for 24 h promotes resistance to both TRAIL- and UMI-77–induced apoptosis as shown in annexin V-FITC staining assays (*H*) and reduced activation of caspase-3 and cleavage of PARP as shown in Western blotting (*I*) ($n = 3$; mean ± SD; Student's *t* test). $^{**}P < 0.01$; $^{***}P < 0.001$.

OVAAL is a lncRNA from the intergenic fragment between *ACBD6* and *XPR1* within a frequently amplified region at chromosome 1q25 in ovarian adenocarcinoma and also in endometrial cancers (34, 35) (*SI Appendix*, Fig. S1*F*). However, its cellular functions have not been previously reported. OVAAL is encoded by three exons (UCSC Genome Browser; *SI Appendix*, Fig. S1*F*) and was readily detectable in ME4405 melanoma cells by Northern blotting (Fig. 1*C*). Consistent with qPCR analysis, up-regulation of OVAAL in TRAIL.S cells and UMI-77.S cells was

confirmed by Northern blotting (Fig. 1*C*). Transduction of three independent OVAAL shRNAs into TRAIL.S and UMI-77.S cells markedly induced apoptosis (Fig. 1 *D* and *E*), along with associated activation of caspase-3 and cleavage of its substrate PARP (Fig. 1*F*). Moreover, recapitulating the acquired resistance phenotype, overexpression of OVAAL in ME4405 cells conferred resistance to both TRAIL- and UMI-77–induced apoptosis (Fig. 1 *G*–*I*).

OVAAL Is Frequently Overexpressed in Colon Cancer and Melanoma and Functions to Promote Cancer Cell Survival and Proliferation. We next expanded our investigations to examine the functions of OVAAL in unselected (parental) cells. Silencing of OVAAL by shRNA in ME4405 melanoma cells, along with HCT116 colon cancer cells, resulted in marked apoptosis as seen by cleavage of caspase-3 and PARP upon TRAIL treatment (Fig. 2*A*). However, knockdown of OVAAL in untransformed human adult foreskin fibroblast (HAFF) cells did not cause cleavage of caspase-3 and PARP upon TRAIL treatment (Fig. 2*B*), suggesting a specific prosurvival role of OVAAL in cancer cells. In addition, OVAAL shRNA inhibited cancer cell proliferation (Fig. 2*C*), which was substantiated through G0/G1 cell cycle arrest (Fig. 2*D*) and decreased phosphorylated Rb (p-Rb), cyclin A, and cyclin B levels and increased cyclin D and cyclin E levels (Fig. 2*E*). In agreement, the growth inhibitory effects of OVAAL knockdown were mirrored in the long-term survival of ME4405 and HCT116 cells as shown in clonogenic assays (Fig. 2*F*). Similarly, OVAAL depletion retarded HCT116 xenograft growth in nu/nu mice (Fig. 2 *G* and *H*). Intriguingly, the presence of OVAAL also protected cancer cells from treatment with venetoclax (ABT-199) and A-1331852, selective inhibitors of Bcl-2 and Bcl-xL, respectively (*SI Appendix*, Fig. S2 *A* and *B*). Taken together, this establishes a role for OVAAL in promoting cancer cell proliferation; moreover, the

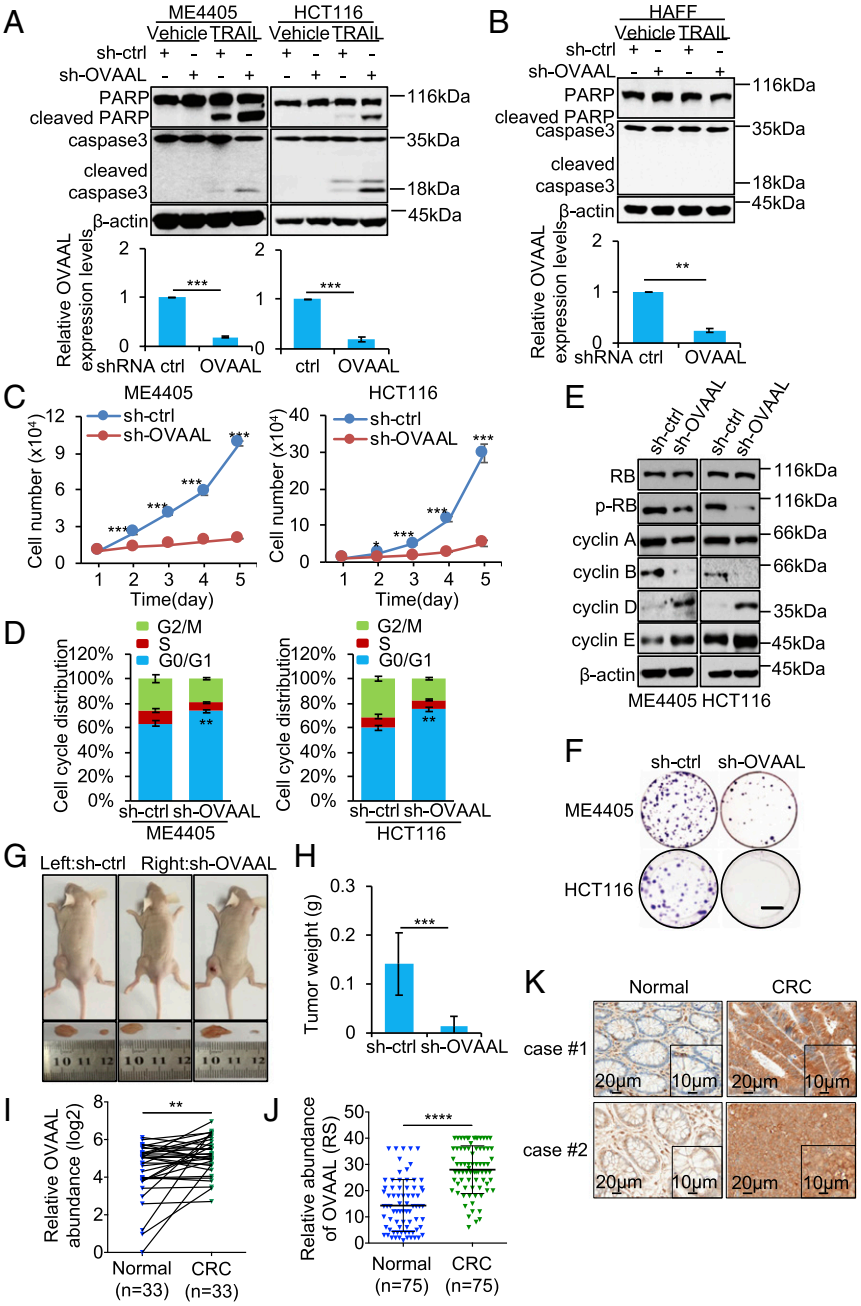

Fig. 2. OVAAL is frequently overexpressed in colon cancer and melanoma, and functions to promote cancer cell survival and proliferation. (*A*, *Top*) As shown in Western blotting, OVAAL shRNA caused enhanced activation of caspase-3 and cleavage of PARP in ME4405 and HCT116 cells treated with vehicle control (ctrl) or TRAIL (200 ng/mL) for 24 h. (*A*, *Bottom*) OVAAL depletion was confirmed by qPCR. β-actin was used as a loading ctrl throughout ($n = 3$; mean ± SD; Student's *t* test). (*B*, *Top*) As shown in Western blotting, OVAAL shRNA did not cause activation of caspase-3 and cleavage of PARP in HAFF cells treated with vehicle ctrl or TRAIL (200 ng/mL) for 24 h. (*B*, *Bottom*) OVAAL depletion was confirmed by qPCR ($n = 3$; mean ± SD; Student's *t* test). (*C*) OVAAL shRNA inhibited cell proliferation in ME4405 and HCT116 cells ($n = 3$; mean ± SD; Student's *t* test). (*D*) OVAAL shRNA caused cell cycle arrest in G0/G1 phase in ME4405 and HCT116 cells measured by propidium iodide staining, followed by flow cytometry ($n = 3$; mean ± SD; Student's *t* test). (*E*) OVAAL shRNA decreased the levels of p-Rb, cyclin A, and cyclin B levels and increased cyclin D and cyclin E levels in ME4405 and HCT116 cells as shown by Western blotting ($n = 3$). (*F*) OVAAL shRNA inhibited cell proliferation in ME4405 and HCT116 cells as shown in colony formation assays ($n = 3$). (Scale bar: 1 cm.) (*G* and *H*) OVAAL depletion by shRNA inhibited HCT116 xenograft growth in nu/nu mice ($n = 7$; mean ± SD; Student's *t* test). (*I*) Measurement of expression using qPCR shows higher levels of OVAAL in CRC compared with paired adjacent normal tissues ($n = 33$; mean ± SD; Student's *t* test). (*J*) Assessment of OVAAL expression using in situ hybridization assays demonstrates significantly increased expressed in CRC in comparison to adjacent normal tissues ($n = 75$; mean ± SD; Student's *t* test) RS, reactive score. (*K*) Representative photomicrographs of OVAAL ISH staining in FFPE tissue samples from *J* showing high differential expression between cancer and normal tissue. $^{**}P < 0.01$; $^{***}P < 0.001$; $^{****}P < 0.0001$.

latter findings suggest a more extensive role for OVAAL in regulating cancer cell survival.

To determine if OVAAL expression was relevant to cancers in vivo, we next considered its expression in clinically derived samples. We employed two analysis approaches to compare the expression of OVAAL between colon cancer tissues and their normal adjacent tissues. First, comparative expression analysis using qPCR showed OVAAL expression was frequently increased in pairs of colorectal cancer (CRC) tissues versus normal adjacent tissues (Fig. 2*I*). Moreover, the application of in situ hybridization to measure OVAAL expression in an independent CRC cohort also revealed significantly increased OVAAL expression in CRC tissues versus normal tissues (Fig. 2*J* and *SI Appendix*, Table S2), a subset of which displayed high differential expression (Fig. 2*K*). Similarly, OVAAL expression was significantly higher in primary melanomas compared with normal nevi displayed in the R2 database (*SI Appendix*, Fig. S3*A*). The differentially increased expression of OVAAL in these cancers therefore suggests its cellular functions may contribute to disease pathology.

OVAAL Interacts with STK3. We hypothesized that like many other regulatory lncRNAs (9, 36, 37), OVAAL acts through direct binding to protein effectors. Hence, we sought to identify the protein interactome of OVAAL using mass spectrometry (37). One prominent target protein selectively pulled down by biotin-labeled antisense probes against OVAAL was identified as STK3, while another was identified as PTBP1 (Fig. 3 *A* and *B*) (as discussed below). Consistently, OVAAL was coimmunoprecipitated by STK3 antibodies by RNA immunoprecipitation (RIP) assays in ME4405 and HCT116 cells (Fig. 3*C*). To further substantiate this interaction, OVAAL was also demonstrated to coprecipitate with STK3 using an overexpression system employing Flag-STK3 and Flag antibodies (Fig. 3*D*). Of interest, significant cytoplasmic and nuclear pools of OVAAL were detected in both ME4405 and HCT116 cells (Fig. 3*E*, *Left*), and this distribution was further confirmed using FISH assays (Fig. 3*F*). Notably, the majority of the STK3 protein in both ME4405 and HCT116 cells was localized to the cytoplasm (Fig. 3*E*, *Right*).

To define which region of OVAAL is responsible for binding to STK3, we first employed a deletion mapping strategy using in vitro-transcribed OVAAL fragments and recombinant Flag-tagged STK3 and deduced that regions within exon 3 (E3) of OVAAL were responsible for STK3 binding (Fig. 3 *G* and *H*). E3 is by far the largest exon in the OVAAL gene (*SI Appendix*, Fig. S1*F*), and subdividing this further demonstrated that the STK3-binding activity was contained with nucleotides 524–824 (Fig. 3*I*).

OVAAL Activates RAF/MEK/ERK Cascade Through Facilitating the Binding Between STK3 and Raf-1. Since the STK3/Raf-1 complex is known to be important for optimal activation of the RAF/MEK/ERK signaling pathway (26), we investigated the potential contribution of OVAAL. Silencing of OVAAL prominently reduced the activation of RAF/MEK/ERK cascade as shown by decreases in p-MEK, p-ERK, p-MSK1, and p-RSK1, recapitulating the effects observed after knockdown of STK3 in ME4405 and HCT116 cells (Fig. 4 *A* and *B*). Instructively, cosilencing of OVAAL in combination with STK3 did not result in further diminishment in RAF/MEK/ERK activation levels, implying that OVAAL-mediated regulation of the RAF/MEK/ERK signaling cascade occurs through effects on STK3 (Fig. 4*C*). Moreover, since STK3 is known to bind to Raf-1 and we identified STK3 as a binding partner of OVAAL, we considered the possibility of a complex formed between OVAAL, STK3, and Raf-1. Indeed, Raf-1, along with STK3, could be coimmunoprecipitated with antisense probes against OVAAL (Fig. 4*D*).

Seeking to further verify the nature of the association between OVAAL, STK3, and Raf-1, we introduced Flag-tagged STK3 into HCT116 cells and used two-step RIP assays. As expected

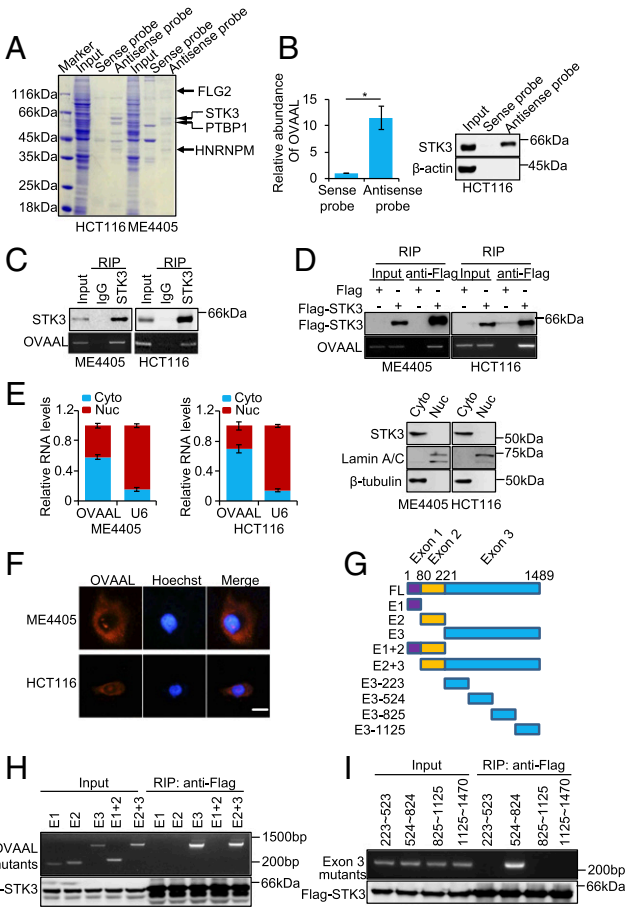

Fig. 3. OVAAL interacts with STK3. (*A*) Visualization of protein bands stained with Coomassie Brilliant Blue pulled down by biotin-labeled antisense probes against OVAAL in total protein extracts of ME4405 and HCT116 cells. Protein identities with high probabilities as determined using mass spectrometry are labeled. (*B*) Biotin-labeled antisense probes used to capture OVAAL from total HCT116 cellular extracts also pulled down by STK3 as shown by qPCR analysis (*Left*) and Western blotting (*Right*) ($n = 3$; mean ± SD; Student's *t* test). *$P < 0.05$. (*C*) Antibodies against STK3 coprecipitated OVAAL from total cellular extracts of ME4405 and HCT116 cells as shown in Western blotting (*Top*) and PCR analysis (*Bottom*) ($n = 3$). (*D*) Anti-Flag (M2) antibodies precipitated OVAAL, along with Flag-STK3, from total ME4405 and HCT116 cellular extracts as shown in Western blotting (*Top*) and PCR analysis (*Bottom*) ($n = 3$). (*E*) Subcellular fractionation studies conducted in ME4405 and HCT116 cells showed that approximately half of OVAAL RNA was located to the cytoplasm, along with the STK3 protein, as shown by qPCR analysis (*Left*) and Western blotting (*Right*) ($n = 3$, mean ± SD). Cyto, cytoplasmic; Nuc, nuclear. (*F*) Subcellular localization of OVAAL was examined by RNA FISH (red) in ME4405 and HCT116 cells. Nuclear DNA was visualized with DAPI (blue). (Scale bar: 20 μm.) (*G*) Schematic representation of OVAAL RNA and the design of exon-deletion constructs used for the analyses shown in *H*. E3 was further was subdivided into four regions for the analyses shown in *I*. (*H* and *I*) Anti-Flag (M2) antibody precipitates from whole-cell lysates of Flag-STK3–transfected HCT116 cells were co-incubated with the indicated in vitro-transcribed OVAAL constructs. RT-PCR analyses (*Top*) were used to detect binding of OVAAL RNA, and Western blotting (*Bottom*) was used to validate input and capture of Flag-STK3 ($n = 3$).

from prior experiments, antibodies against the Flag-tag precipitated STK3, along with Raf-1 and OVAAL, from total protein extracts (Fig. 4*E*, *Left*), while in the second-phase immunoprecipitation using anti–Raf-1 antibodies, both STK3 and OVAAL were coprecipitated (Fig. 4*E*, *Right*). Instructively, knockdown of OVAAL abolished the binding between Raf-1 and STK3 (Fig. 4*F*), thereby implying that OVAAL is required for the interaction between STK3 and Raf-1. Indeed, the application of a cell-free

system demonstrated that OVAAL promoted increased binding between purified STK3 and Raf-1 (Fig. 4*G*). Moreover, phosphorylation of Raf-1 at serine 259, an inhibitory phosphorylation of Raf-1 (38), was increased by OVAAL knockdown (Fig. 4*H*) similar to the effects of STK3 knockdown (Fig. 4*I*), suggesting OVAAL and STK3 promote Raf-1 activation through its phosphorylation. Together, these findings support the notion that OVAAL directly facilitates assembly of a ternary complex with STK3/Raf-1 and that this complex promotes downstream activation of RAF/MEK/ERK signaling.

Finally, of relevance to these results, OVAAL expression levels were frequently higher in metastatic melanomas bearing the $BRAF^{V600}$ mutant compared with wild-type BRAF melanomas from The Cancer Genome Atlas (TCGA) dataset (*SI Appendix*, Fig. S3*B*), suggesting a correlation between high OVAAL expression and MAPK pathway activation. Of interest, OVAAL silencing further reduced cancer cell viability upon MEK inhibitor treatment, suggesting a central role for OVAAL in RAF/MEK/ERK signaling (*SI Appendix*, Fig. S3*C*).

OVAAL Promotes Cell Proliferation via Stabilization of c-Myc. Activation of the RAF/MEK/ERK pathway is important for up-regulation of c-Myc, a critical regulator of cancer cell survival and proliferation (31, 39, 40). Similar to knockdown of STK3, OVAAL shRNA significantly reduced c-Myc protein expression levels (Fig. 5 *A* and *B*). Moreover, reduction of c-Myc expression by OVAAL shRNA was rescued by an shRNA-resistant OVAAL (Fig. 5*C*). Conversely, overexpression of OVAAL in HCT116 cells resulted in increased c-Myc protein levels (Fig. 5*D*), collectively indicating that OVAAL promotes increased c-Myc expression. Notably, suppression of the RAF/MEK/ERK pathway using the MEK inhibitor U0126 ablated the expression of c-Myc, and overexpression of OVAAL under these conditions failed to influence the levels of c-Myc (*SI Appendix*, Fig. S4*A*), suggesting that the OVAAL-mediated up-regulation of c-Myc depends on RAF/MEK/ERK pathway.

We further investigated the mechanism by which OVAAL up-regulated c-Myc protein levels. The c-Myc mRNA levels were not affected by either OVAAL shRNA or STK3 shRNA (*SI Appendix*, Fig. S4*B*). However, the proteasome inhibitor MG132 stabilized c-Myc protein levels, reversing the effects of OVAAL silencing (Fig. 5*E*). Surprisingly, knockdown of OVAAL did not result in the expression levels of two known c-Myc E3 ligases: SKP2 and FBXW7 (*SI Appendix*, Fig. S4*C*). Nevertheless, knockdown of either OVAAL or STK3 shortened the half-life of c-Myc protein (Fig. 5*F*), suggesting that OVAAL enhances c-Myc protein stability by preventing its degradation through the proteasome pathway (41–43). Strengthening this notion, depletion of OVAAL increased the levels of c-Myc ubiquitination (Fig. 5*G*), along with causing decreased levels of Ser62 phosphorylation of c-Myc, a post-translational modification (PTM) associated with stabilization of the c-Myc protein (Fig. 5*H*). Collectively, these findings indicate that the OVAAL-mediated effects on c-Myc protein levels are enacted through changes in protein stability.

Given the regulatory relationship established between OVAAL and the maintenance of the cellular levels of c-Myc, we then returned to examine the contribution of c-Myc to the functions of OVAAL. Surprisingly, unlike OVAAL depletion, silencing of c-Myc was insufficient to sensitize ME4405 and HCT116 cells to apoptosis after TRAIL treatment (*SI Appendix*, Fig. S4*D*), suggesting that c-Myc is not required for OVAAL-mediated inhibition of apoptosis. Nevertheless, besides its apoptosis-inducing capacity upon TRAIL treatment, knockdown of OVAAL also inhibited cell proliferation (Fig. 2 *C*–*F*). The results support the concept that OVAAL expression plays an important role in cancer cell proliferation and these actions are imparted through effects on c-Myc expression.

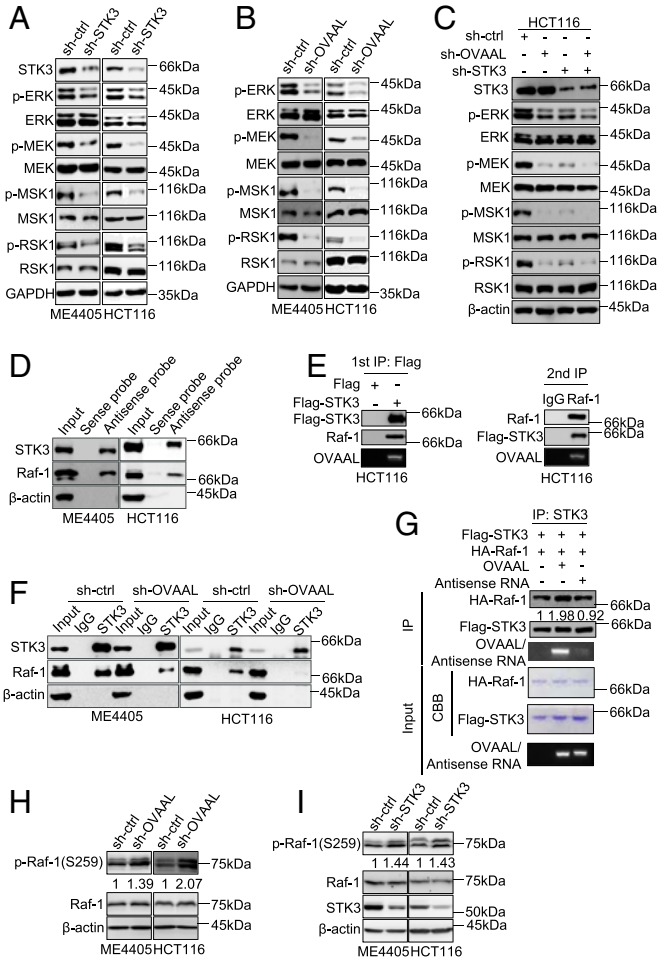

Fig. 4. OVAAL activates RAF/MEK/ERK cascade through facilitating the binding between STK3 and Raf-1. (*A*) STK3 shRNA decreased levels of p-ERK, p-MEK, p-MSK1, and p-RSK1 in ME4405 and HCT116 cells as shown in Western blotting. Analysis of total ERK, MEK, MSK1, and RSK1, along with a GAPDH loading control (ctrl), is shown for comparison ($n = 3$). (*B*) OVAAL shRNA decreased levels of p-ERK, p-MEK, p-MSK1, and p-RSK1 in ME4405 and HCT116 cells as shown in Western blotting ($n = 3$). (*C*) Co-silencing of OVAAL with STK3 in HCT116 cells did not impart further reductions in the phosphorylated levels of ERK, MEK, MSK1, or RSK1 levels in comparison to STK3 knockdown alone as measured by Western blotting ($n = 3$). (*D*) Biotin-labeled antisense probes used to capture OVAAL from total cellular lysates of ME4405 and HCT116 cells also pulled down STK3, along with Raf-1, as shown by Western blotting. β-Actin was used as a negative ctrl here and in the following experiments ($n = 3$). (*E*) Flag-STK3, Raf-1, and OVAAL were coprecipitated with an anti-Flag antibody in whole-cell lysates of HCT116 cells transfected with Flag-STK3 (*Left*), and after elution with Flag peptide, all were further coprecipitated with an anti–Raf-1 antibody in the resultant precipitates (*Right*). IP, immunoprecipitation. (*F*) OVAAL depletion strongly diminished the levels of Raf-1 associating with STK3. Endogenous STK3 was immunoprecipitated from sh-ctrl– or sh-OVAAL–treated ME4405 and HCT116 cells, with results shown by Western blotting ($n = 3$). (*G*) Presence of in vitro-transcribed OVAAL, but not an antisense RNA, enhanced the binding between recombinant HA–Raf-1 and Flag-STK3. Assay inputs were visualized by Coomassie Brilliant Blue (CBB) and ethidium bromide staining ($n = 3$). OVAAL shRNA (*H*) and STK3 shRNA (*I*) increased levels of p-Raf-1 (Ser259) in ME4405 and HCT116 cells as shown in Western blotting ($n = 3$).

OVAAL Counteracts TRAIL- and UMI-77–Induced Apoptosis Through Up-Regulation of Mcl-1. The preceding experiments demonstrate how OVAAL promotes cell proliferation, but the mechanism whereby OVAAL protects cancer cells from apoptosis appears to be distinct. Instructively, when OVAAL shRNA was introduced into ME4405 cells, among the prosurvival Bcl-2 family members,

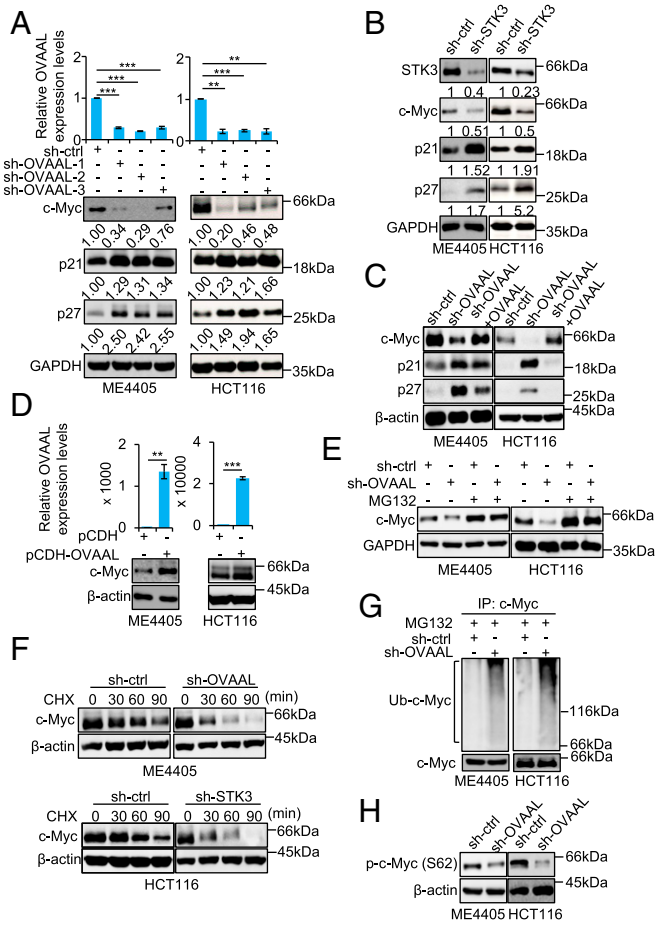

Fig. 5. OVAAL promotes cell proliferation via stabilization of c-Myc. (*A*) OVAAL shRNA reduced c-Myc and increased p21 and p27 protein expression levels in ME4405 and HCT116 cells as shown in qPCR analyses (*Top*) and Western blotting (*Bottom*). GAPDH or β-actin is used throughout as a loading control (ctrl) ($n = 3$; mean ± SD; Student's *t* test). (*B*) STK3 shRNA reduced c-Myc and increased p21 and p27 protein expression levels in ME4405 and HCT116 cells as shown in Western blotting ($n = 3$). (*C*) Reductions in c-Myc expression following OVAAL shRNA are rescued by overexpression of OVAAL in ME4405 and HCT116 cells as shown in Western blotting ($n = 3$). (*D*, *Bottom*) As shown in Western blotting, overexpression of OVAAL increased c-Myc protein expression levels in ME4405 and HCT116 cells. (*D*, *Top*) Analysis of total RNA by qPCR analysis confirmed the increase in OVAAL expression in cells transduced with pCDH-OVAAL compared with the control pCDH vector ($n = 3$; mean ± SD; Student's *t* test). (*E*) Treatment of ME4405 and HCT116 cells with the proteasome inhibitor MG132 (50 μM) reversed the decrease in c-Myc protein levels resulting from silencing of OVAAL as shown in Western blotting ($n = 3$). (*F*) shRNA silencing of either OVAAL (*Top*) or STK3 (*Bottom*) shortened the half-life of c-Myc protein in cycloheximide chase assays ($n = 3$). (*G*) OVAAL shRNA increased c-Myc polyubiquitination levels in the presence of MG132 (50 μM) ($n = 3$). IP, immunoprecipitation. (*H*) OVAAL shRNA reduced phosphorylated c-Myc (Ser62) levels in ME4405 and HCT116 cells as shown in Western blotting ($n = 3$). $^{**}P < 0.01$; $^{***}P < 0.001$.

Mcl-1 protein expression levels were most prominently reduced (Fig. 6*A*). Moreover, inhibition of RAF/MEK/ERK cascade by the MEK inhibitor U0126 caused the reduction of Mcl-1 expression in TRAIL.S cells (Fig. 6*B*). Similar to knockdown of OVAAL, silencing of STK3 reduced Mcl-1 expression, implying loss of balance between cell survival and apoptosis (Fig. 6*C*). Similar to knockdown of OVAAL, depletion of Mcl-1 itself also augmented the apoptotic effects of TRAIL and UMI-77 (Fig. 6*D*), implying that Mcl-1 contributes to the OVAAL-derived resistance to TRAIL- and UMI-77–induced apoptosis. Finally, overexpression of Mcl-1 served to diminish OVAAL depletion-enhanced apoptosis under TRAIL treatment (Fig. 6*E*), suggesting a Mcl-1–dependent prosurvival role of OVAAL in cancer cells. Instructively, inhibition of proteasomal activity using MG132 reversed the decrease in Mcl-1 protein levels observed after OVAAL silencing (Fig. 6*F*). Moreover, knockdown of OVAAL shortened the half-life time of Mcl-1 protein (Fig. 6*G*), suggesting that OVAAL enhances Mcl-1 protein stability through a proteasome pathway. In support, phosphorylation of Mcl-1 at threonine 163, known to be mediated by ERK and to slow Mcl-1 protein turnover, was reduced after OVAAL silencing (Fig. 6*H*).

OVAAL Blocks Cellular Senescence by Regulating p27 mRNA Translation. Given the observation that silencing of OVAAL resulted in up-regulation of the CDK inhibitors p21 and p27 (Fig. 5*A*), we further considered if these cells were entering senescence. Indeed, depletion of OVAAL also triggered cellular senescence as shown by induction of senescence-associated (SA)–ß-gal staining (44, 45) (Fig. 7*A*). Of interest, mass spectrometry data showed that PTBP1, an RNA-binding protein known to bind to an IRES element in the

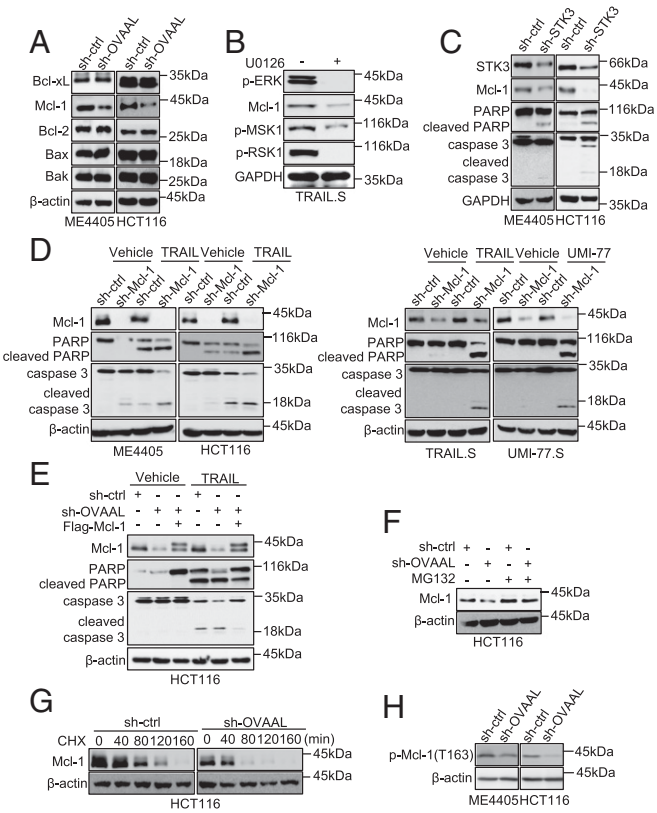

Fig. 6. OVAAL counteracts TRAIL- and UMI-77–induced apoptosis through up-regulation of Mcl-1. (*A*) OVAAL shRNA decreased levels of Mcl-1 in ME4405 and HCT116 cells as shown in Western blotting ($n = 3$). ctrl, control. (*B*) MEK inhibitor U0126 (10 μM) caused the reduction of Mcl-1 expression in TRAIL.S cells as shown in Western blotting ($n = 3$). (*C*) STK3 shRNA reduced Mcl-1 expression and increased activation of caspase-3 and cleavage of PARP in ME4405 and HCT116 cells as shown in Western blotting ($n = 3$). (*D*) Mcl-1 shRNA enhanced activation of caspase-3 and cleavage of PARP in ME4405, HCT116, TRAIL.S, and UMI-77.S cells treated with vehicle ctrl, TRAIL, or UMI-77 for 24 h as shown in Western blotting ($n = 3$). (*E*) Overexpression of Mcl-1 diminished OVAAL depletion-increased cleavage of caspase-3 and PARP under TRAIL (50 ng/mL) treatment in HCT116 cells ($n = 3$). (*F*) Proteasome inhibitor MG132 (50 μM) reversed the decrease in Mcl-1 protein levels by OVAAL silencing in HCT116 cells as shown in Western blotting ($n = 3$). (*G*) OVAAL shRNA shortened the half-life of Mcl-1 protein in HCT116 cells as shown in Western blotting ($n = 3$). (*H*) OVAAL shRNA reduced p-Mcl-1 (Thr163) levels in ME4405 and HCT116 cells as shown in Western blotting ($n = 3$).

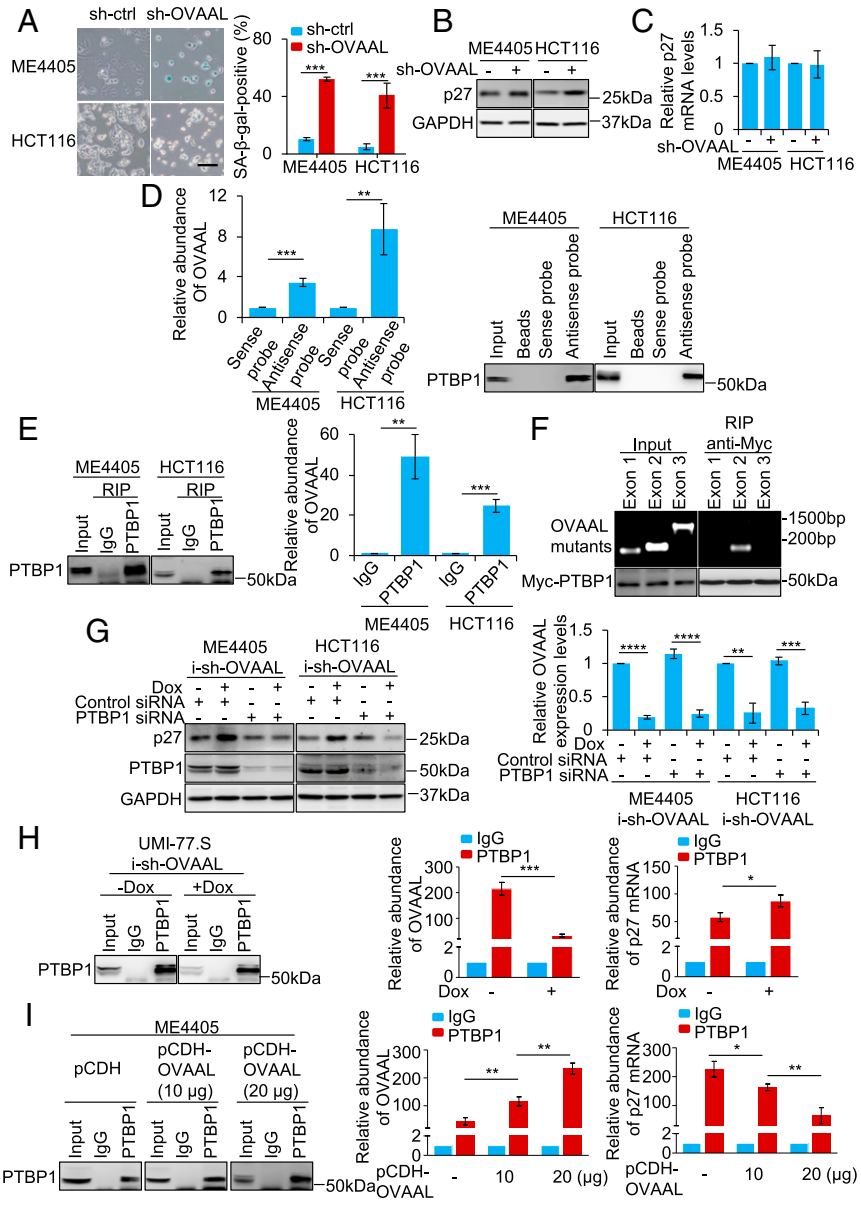

Fig. 7. OVAAL blocks cellular senescence via regulation of p27 translation. (*A*) OVAAL shRNA triggered cellular senescence as shown by induction of SA–β-gal staining in ME4405 and HCT116 cells. Representative photographs (*Left*) and quantification of staining (*Right*) are shown ($n = 3$; mean ± SD; Student's t test). ctrl, control. (Scale bar: 200 μm.) (*B*) OVAAL shRNA increased the levels of p27 protein in ME4405 and HCT116 cells as shown in Western blotting ($n = 3$). (*C*) OVAAL shRNA did not affect p27 mRNA levels in ME4405 and HCT116 cells as shown in qPCR analysis ($n = 3$; mean ± SD). (*D*) Biotin-labeled antisense probes against OVAAL pulled down OVAAL, along with PTBP1, from total ME4405 and HCT116 cellular extracts as shown in qPCR analysis (*Left*) and Western blotting (*Right*) ($n = 3$; mean ± SD; Student's t test). (*E*) Antibody against PTBP1 precipitated PTBP1, along with OVAAL, from total ME4405 and HCT116 cellular extracts as shown in Western blotting (*Left*) and qPCR analysis (*Right*) ($n = 3$; mean ± SD; Student's t test). (*F*) Myc-tag antibody precipitated Myc-PTBP1 from HCT116 whole-cell lysates, along with co-incubated in vitro-transcribed mutant OVAAL, as shown in PCR analysis (*Top*) and Western blotting (*Bottom*) ($n = 3$). (*G*) Cosilencing of PTBP1 abolished the up-regulation of p27 protein following OVAAL knockdown in parental ME4405 and HCT116 cells bearing an inducible knockdown system (i-sh-OVAAL) activated with doxycycline (Dox; 100 ng/mL). Results are shown in Western blotting (*Left*) and qPCR analysis (*Right*) ($n = 3$; mean ± SD; Student's t test). (*H*) Depletion of OVAAL following Dox (100 ng/mL) treatment increased the association between PTBP1 and p27 mRNA in OVAAL-inducible knockdown UMI-77.S cells (UMI-77.S i-sh-OVAAL). PTBP1 immunoprecipitates were assessed using Western blotting (*Left*) and qPCR analysis (*Right*) ($n = 3$; mean ± SD; Student's t test). (*I*) Overexpression of OVAAL in a dose-dependent manner decreased the association between PTBP1 and p27 mRNA in ME4405 cells. Analysis as per *H* is shown using Western blotting (*Left*) and qPCR (*Right*) ($n = 3$, mean ± SD; Student's t test). *$P < 0.05$; **$P < 0.01$; ***$P < 0.001$; ****$P < 0.0001$.

5′ UTR of p27 mRNA and to promote p27 translation (29), was a putative binding partner of OVAAL (Fig. 3*A*). Further examination of the relationship between OVAAL and p27 expression showed that the increased p27 protein levels (Fig. 7*B*) observed after silencing of OVAAL did not increase p27 mRNA levels (Fig. 7*C*), thereby suggesting that OVAAL regulates cellular senescence via controlling p27 protein expression levels.

The interaction between PTBP1 and OVAAL was confirmed by RNA pulldown (Fig. 7*D*) and RIP (Fig. 7*E*), respectively. Further analyses demonstrated that only RNA transcripts containing E2 of OVAAL bound to the PTBP1 protein (Fig. 7*F*). Noticeably, the increased p27 protein levels accompanying OVAAL knockdown could be reversed by cosilencing of PTBP1, implying that PTBP1 is necessary for OVAAL-mediated p27 protein expression (Fig. 7*G*). Together, this implied that OVAAL competes with p27 mRNA for binding to PTBP1. Consistent with this proposition, more p27 mRNA was associated with PTBP1 when OVAAL levels were reduced in cells bearing an OVAAL-inducible knockdown system (Fig. 7*H*). Conversely, overexpression of OVAAL by transfection resulted in a dose-dependent increase in OVAAL association with PTBP1, while the levels of recovered p27 decreased (Fig. 7*I*).

c-Myc Transcriptionally Regulates OVAAL in Cancer Cells. Using in silico analysis, we identified two putative c-Myc–binding sites (c-Myc–BS1: −2,603 to −2,595 bp and c-Myc–BS2: −1,585 to −1,551 bp) upstream of the *OVAAL* transcriptional start site (Fig. 8*A*). Luciferase reporter assays showed both regions were responsible for c-Myc–mediated OVAAL transcription (Fig. 8*B*). Moreover, ChIP analyses confirmed that c-Myc bound to both of the identified binding sites in the *OVAAL* promoter (Fig. 8*C*). In agreement, silencing of c-Myc reduced, whereas overexpression of c-Myc increased, the expression levels of OVAAL (Fig. 8 *D* and *E*). The application of an independent cell system involving P493-6 cells carrying a c-Myc tet-off system also confirmed the dependency of OVAAL expression on c-Myc levels (Fig. 8*F*). Consistently, c-Myc expression levels were also up-regulated in TRAIL.S cells that exhibit increased OVAAL expression relative to their parental cells (Fig. 8*G*).

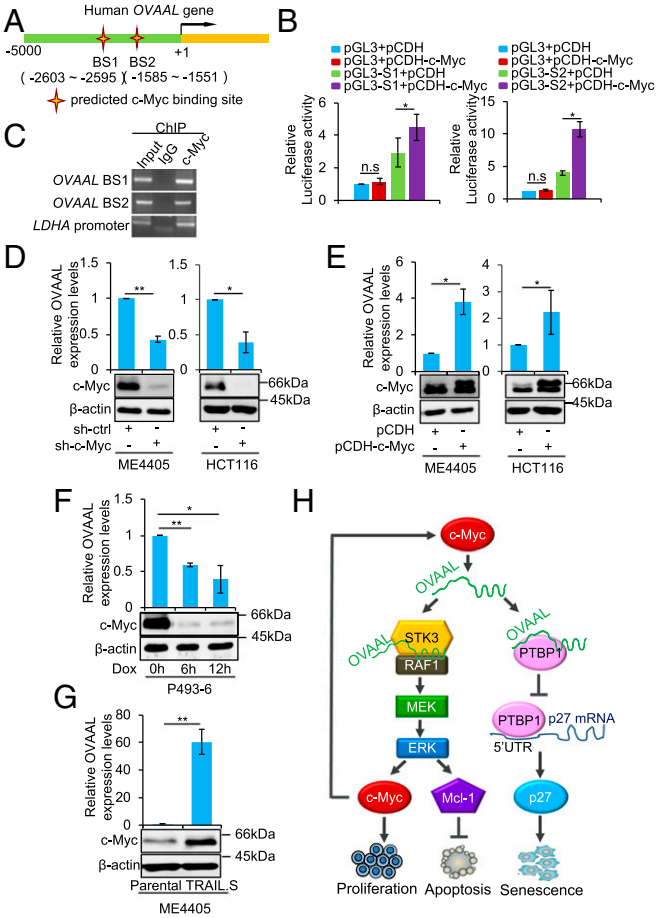

Fig. 8. c-Myc transcriptionally regulates OVAAL in cancer cells. (*A*) Two potential c-Myc–binding sites in the *OVAAL* promoter region were predicted in the high-quality transcription factor binding profile database (JASPAR). (*B*) Both predicted regions were transcriptionally responsive to c-Myc overexpression as shown in luciferase reporter assays ($n = 3$; mean ± SD; Student's *t* test). (*C*) c-Myc bound to both predicted c-Myc–binding sites in *OVAAL* promoter as shown in ChIP assays. Lactate dehydrogenase A (LDHA) promoter was used as a positive control ($n = 3$). (*D*) c-Myc shRNA reduced the levels of OVAAL in ME4405 and HCT116 cells as shown in qPCR analysis (*Top*) and Western blotting (*Bottom*) ($n = 3$; mean ± SD; Student's *t* test). ctrl, control. (*E*) Overexpression of c-Myc increased the expression levels of OVAAL in ME4405 and HCT116 cells as shown in qPCR analysis (*Top*) and Western blotting (*Bottom*) ($n = 3$; mean ± SD; Student's *t* test). (*F*) Expression levels of OVAAL in P493-6 cells carrying a c-Myc tet-off system were decreased when cells were treated with doxycycline (Dox; 1 μM) as shown in qPCR analysis (*Top*) and Western blotting (*Bottom*) ($n = 3$; mean ± SD; Student's *t* test). (*G*) c-Myc, along with OVAAL, was up-regulated in TRAIL.S cells in comparison to ME4405 cells as shown in qPCR analysis (*Top*) and Western blotting (*Bottom*) ($n = 3$; mean ± SD; Student's *t* test). (*H*) Schematic illustration of proposed model depicting dual roles of lncRNA OVAAL in regulating cell proliferation/apoptosis and senescence. $^*P < 0.05$; $^{**}P < 0.01$.

Discussion

The RAS/RAF/MAPK pathway is hyperactivated in ∼30% of human cancers (46, 47), where its activating mutations, such as $BRAF^{V600E}$ and $H\text{-}RAS^{V12H}$, are driver mutations in many malignancies (48, 49). When the RAF/MEK/MAPK pathway is aberrantly activated in normal cells, they are induced to undergo apoptosis, cell cycle arrest, and/or cellular senescence, which serves to limit cell transformation and tumor progression (50, 51). Consequently, overcoming these major intrinsic failsafe mechanisms is a key permissive step in tumorigenesis (46). In this study, we sought to identify lncRNAs expressed by cancer cells that facilitate resistance to apoptosis, using cell line models adapted to overcome TRAIL- and UMI-77–induced apoptosis. We report here that OVAAL protects cancer cells from apoptosis and that this function was integrally linked to the enhanced activation of the RAS/RAF/MAPK pathway. Of likely importance, OVAAL is commonly overexpressed in colon cancer and melanoma, particularly in BRAF mutant melanoma (Fig. 2 *I–K* and *SI Appendix*, Fig. S3 *A* and *B*), suggesting up-regulation of OVAAL may contribute to tumorigenesis. Moreover, OVAAL expression is driven by c-Myc, and it promotes cell proliferation via a feedback control over c-Myc stability and inhibits cellular senescence via targeting p27 mRNA translation. Of importance, OVAAL significantly protected cancer cells from death triggered by MEK inhibition, indicating that OVAAL plays a central role in RAF/MEK/ERK prosurvival signaling (*SI Appendix*, Fig. S3*C*).

Our approach sought to find intersections between the two major apoptotic signaling pathways (52, 53): the death receptor-mediated "extrinsic apoptotic pathway" and the mitochondrion-mediated "intrinsic apoptotic pathway." Although a number of lncRNAs were found to be highly up-regulated in melanoma cells resistant to TRAIL (extrinsic apoptotic pathway) and/or the Mcl-1 inhibitor UMI-77 (intrinsic apoptotic pathway), of those tested, only OVAAL protected cells from death in both cell line models. Silencing of OVAAL resensitized cancer cells to TRAIL or UMI-77 treatment, which was closely associated with a reduction in the stability of Mcl-1 protein. The importance of OVAAL as a crucial regulator allowing cancer cells to escape apoptosis is borne out in experiments with other cancer cell types, where inhibiting OVAAL sensitized cells to TRAIL-mediated apoptosis. We also observed that expression of OVAAL by selected and naive cells alike protected against treatment with specific inhibitors of Bcl-2 and Bcl-xL. Although a clear relationship was established between OVAAL and the stabilization of Mcl-1 through inhibition of proteasomal degradation, we did not fully investigate how these Mcl-1–related genes were controlled by OVAAL, and it will be pertinent to define this in future studies.

STK3, also known as MST2, is a major kinase regulating the Hippo pathway (54). However, in contrast to the effects of silencing of STK3, depleting OVAAL failed to reduce Ser127 phosphorylation of YAP1 (55), an indicator of Hippo pathway activation, suggesting that OVAAL does not influence Hippo signaling in this context (*SI Appendix*, Fig. S5). Our finding that OVAAL enhances the association between STK3 and Raf-1 thereby suggests that OVAAL might promote cancer cell survival and proliferation in two ways. First, by stabilizing the interaction between STK3 and Raf-1, this would inhibit STK3 association with RASSF1A, thus blocking STK3-mediated apoptosis. Second, the stabilized STK3/Raf-1 complex would accentuate activation of the RAF/MEK/ERK signal pathway. Given that relatively high levels of OVAAL appear to be necessary for Raf-1 to associate with STK3, we have established the latter, but more experiments are required to address whether high levels of OVAAL serve to disrupt the interaction between STK3 and RASSF1A and prevent apoptosis. Nevertheless, these findings promote the potential for antagonizing OVAAL as a means to inhibit growth in tumors hyperactivated by RAF/MEK/ERK signaling.

A second significant finding concerns the functional role of OVAAL in senescence. Senescence is typically induced by unrepaired DNA damage or following other cellular stresses, such as abnormal activation of oncogenes, thus leading to suppression of tumorigenesis (56–58). For instance, the expression of $BRAF^{V600E}$ in cultured primary human melanocytes hyperactivates the MEK/ERK cascade accompanied by the induction of senescence (59). Many chemotherapeutic drugs can trigger senescence, proposing a positive contribution of senescence to the success of cancer chemotherapy (58, 60). However, the capacity for senescence appears to be lost in cancer (56, 61), although not totally, since, for example, the BRAF inhibitor encorafenib (LGX818) induced cellular senescence in $BRAF^{V600E}$ mutant melanomas (62). Here, we established that silencing of OVAAL was sufficient to induce cellular senescence in

the absence of any additional treatment. Further, we established that OVAAL functions in this capacity by regulating the expression of p27. Regulation occurs at the translational level, where sequences within E2 of OVAAL bind to PTBP1, which, in turn, prevents PTBP1 from augmenting p27 translation. Given that cellular senescence can have therapeutic benefits, such as triggering innate immune responses to clear senescent cells (63), the induction of senescence may be a second major action resulting from antagonizing OVAAL.

Finally, our study provides significant insights into the regulatory relationship between OVAAL and c-Myc, the "master regulator" whose aberrant expression is commonly associated with tumorigenesis, cell growth, and self-renewal (64, 65). OVAAL was shown to be subject to transcriptional regulation by c-Myc with two active binding motifs localized to the *OVAAL* promoter. However, there is also a feedback loop whereby OVAAL regulates c-Myc posttranslationally through the stabilization of c-Myc protein levels. Moreover, while the inhibitory role of OVAAL in the inhibition of apoptosis appears to be uncoupled from c-Myc, the role of OVAAL in cell proliferation and evasion of senescence involves c-Myc.

The expression of c-Myc is tightly controlled by multiple mechanisms, such as regulation of gene transcription, mRNA translation, and protein stability (66, 67). In particular, phosphorylation at serine 62 by ERK positively regulates, whereas phosphorylation at threonine 58 by GSK3β negatively controls, c-Myc protein stability in response to RAF/MEK/ERK signal transduction (66). Here, we reveal that knockdown of OVAAL inhibits the RAF/MEK/ERK pathway, which, in turn, reduces c-Myc phosphorylation at serine 62 and subsequently causes its degradation. Of note, c-Myc protein is well known to be ubiquitinated and degraded via complexes containing the FBXW7 or SKP2 E3 ligase (68). We observed that silencing of OVAAL was associated with decreased c-Myc protein turnover, along with increased levels of c-Myc polyubiquitination, indicative that OVAAL acts to stabilize c-Myc through control over its proteasomal degradation. However, there were no changes in the protein levels of FBWX7 and SKP2, implying that OVAAL may regulate c-Myc protein stability through another E3 ubiquitin ligase. Notwithstanding knowledge of how OVAAL regulates c-Myc protein stability, the pleiotropic roles of OVAAL in cell growth and resistance to apoptosis in tumors with RAF/MEK/ERK hyperactivation, together with functional effects on senescence in c-Myc–amplified tumors, may provide new opportunities in the treatment of cancer (Fig. 8*H*). Whether targeting OVAAL directly in vivo is practicable remains to be explored. Identification of compounds that block the interaction between OVAAL and STK3 is one avenue to explore, and targeting the cellular levels of OVAAL may be another avenue to target c-Myc, which is considered to be "undruggable" (69).

Materials and Methods

Cell Lines and Tissues. ME4405, TRAIL.S, UMI-77.S, HCT116, P493-6, and HAFF cells were maintained in DMEM (Invitrogen) supplemented with 10% FBS and 1% penicillin/streptomycin. Cells were cultured in a humidified incubator at 37 °C and 5% CO_2. All cell lines used tested negative for mycoplasma contamination and were subjected to authentication using the AmpFISTR Identifiler PCR Amplification Kit (Applied Biosystems) and GeneMarker V1.91 software (SoftGenetics LLC) (70). Formalin-fixed paraffin-embedded (FFPE) colon cancer tissues were obtained from the Department of Pathology at Shanxi Cancer Hospital and Institute (Taiyuan, China). Freshly removed colon cancer and paired adjacent noncancerous colon tissues were collected from patients undergoing surgical resection at the Department of General Surgery at Shanxi Cancer Hospital and Institute. Studies using human tissues were approved by the Human Research Ethics Committees of the University of Science and Technology of China and Shanxi Cancer Hospital and Institute in agreement with the guidelines set forth by the Declaration of Helsinki. The study is compliant with all relevant ethical regulations for human research participants, and all participants provided written informed consent.

Antibodies and Reagents. Antibodies and reagents used are listed in *SI Appendix*, Tables S3 and S4.

Mass Spectrometry. The eluted proteins from OVAAL RNA pulldown assay were identified using a gel-based liquid chromatography-tandem mass spectrometry approach (71). A Mascot database search was used to visualize and validate results.

Biotin RNA Pulldown Assay. The RNA pulldown assay was performed as previously described (72). In brief, all processes were performed in the RNase-free conditions. Briefly, approximately 1×10^7 to 2×10^7 cells were lysed in 1.0 mL of lysis buffer [50 mM Tris·HCl (pH 7.5), 150 mM NaCl, 2.5 mM $MgCl_2$, 1 mM EDTA, 10% glycerol, 0.5% Nonidet P-40, 1 mM DTT, 1 U/μL SUPERase in TM RNase Inhibitor (20 U/μL; Ambion), cOmplete Protease Inhibitor Mixture (Roche)]. Cell lysates were incubated with streptavidin beads (Invitrogen) coated with the biotin-labeled antisense probes (3 μg) at 4 °C for 4 h to overnight. A biotin-labeled sense probe (3 μg) sample was taken as a negative control. Beads were washed five times in RIP buffer and eluted in Laemmli buffer. The retrieved proteins were separated by SDS/PAGE for mass spectrometry or Western blotting.

RIP. RIP was performed with an EZ-Magna RIP Kit (17-701; Millipore) according to the instructions provided by the manufacturer. Briefly, approximately 1×10^7 to 3×10^7 cells were lysed in hypotonic buffer supplemented with RNase inhibitor and protease inhibitor before centrifugation. Cell lysates were incubated with magnetic beads coated with the indicated antibodies at 4 °C for 4 h to overnight. After extensive washing using RIP wash buffer, the bead-bound immunocomplexes were treated with proteinase K at 55 °C for 30 min. To isolate RNAs, samples were centrifuged and placed on a magnetic separator, and supernatants were used to extract RNA by an ISOLATE II RNA Mini Kit (Bioline). Purified RNAs were then subjected to PCR analysis.

RNA Interference. Gene knockdown with shRNA was performed as previously described (73). Briefly, HEK293T cells were transfected with shRNAs (cloned in pLKO.1), gag/pol, rev, and VSVG plasmids with a ratio of 2:2:2:1. Twenty-four hours after transfection, cells were cultured in fresh medium for an additional 24 h. The culture medium containing lentivirus particles was centrifuged at 1,000 × *g* for 5 min, and the supernatant was used for infection. The shRNA sequences are shown in *SI Appendix*, Table S5.

qPCR Analysis. qPCR analyses were conducted as described previously (74). Briefly, total cellular RNA isolated using the ISOLATE II RNA Mini Kit was subject to reverse transcription using qScript cDNA Supermix (Quantabio). Reactions (20 μL) were prepared on ice using SensiFAST SYBR Hi-ROX Kit (Bioline) reagents in combination with the primers listed in *SI Appendix*, Table S6, and cycling was performed for 40 cycles at 95 °C (15 s) and at 60 °C (1 min). The $2^{-\Delta\Delta CT}$ method was used to calculate the relative gene expression levels in comparison to the β-actin housekeeping control.

ChIP Assays. ChIP assays were performed using a Millipore ChIP kit (17-371RF; Millipore) according to the manufacturer's instructions. Bound DNA fragments were subjected to qPCR using the specific primers shown in *SI Appendix*, Table S7.

In Situ Hybridization. FFPE tissue sections (5 μm thick) were deparaffinized, followed by treatment with 10% hydrogen peroxide and pepsin (2 μg/mL; EXIQON) for 1 h at 37 °C. Sections were subsequently prehybridized with hybridization buffer for 1 h at 37 °C before incubation with digoxigenin (DIG)-labeled probes at 37 °C for 24 h (10 μg/mL). Following hybridization, sections were sequentially washed for 10 min using 5× SSC (Gibco), 2× SSC, and 0.2× SSC at 55 °C before equilibrating in blocking buffer (PBS with Tween 20 with 10% normal goat serum and 5% BSA) at 37 °C for 1 h. Sections were then incubated with HRP-conjugated anti-DIG antibody (Abcam) at 4 °C for 12 h; after washing, DAB substrate was applied and counterstaining was performed using hematoxylin solution. After the sections were dehydrated and mounted, they were digitally scanned and staining was quantitated as reactive scores as previously described (75). Probe sequences are shown in *SI Appendix*, Table S7.

Statistical Analysis. Statistical analysis was carried out using Microsoft Excel software and GraphPad Prism to assess differences between experimental groups. Statistical significance was analyzed by a two-tailed Student's *t* test. *P* values less than 0.05 were considered to be statistically significant: $*P < 0.05$, $**P < 0.01$, $***P < 0.001$, and $****P < 0.0001$.

ACKNOWLEDGMENTS. We thank Dr. Marco J. Herold (Walter and Eliza Hall Institute of Medical Research) for providing FH1t (BsmB1) UTG plasmid. This work was supported by grants from the National Key R&D Program of China (Grants 2018YFA0107103 and 2016YFC1302302), National Natural Science Foundation of China (Grants 81820108021,81430065 and 31871437), and National Health and Medical Research Council of Australia (Grants APP1083496 and APP1099947). L.J. is the recipient of a Cancer Institute NSW Fellowship.

1. Kung JT, Colognori D, Lee JT (2013) Long noncoding RNAs: Past, present, and future. *Genetics* 193:651–669.
2. Huarte M (2015) The emerging role of lncRNAs in cancer. *Nat Med* 21:1253–1261.
3. Huang JZ, et al. (2017) A peptide encoded by a putative lncRNA HOXB-AS3 suppresses colon cancer growth. *Mol Cell* 68:171–184.e6.
4. Ruiz-Orera J, Messeguer X, Subirana JA, Alba MM (2014) Long non-coding RNAs as a source of new peptides. *eLife* 3:e03523.
5. Wang JZ, Xu CL, Wu H, Shen SJ (2017) LncRNA SNHG12 promotes cell growth and inhibits cell apoptosis in colorectal cancer cells. *Braz J Med Biol Res* 50:e6079.
6. Ma C, et al. (2014) H19 promotes pancreatic cancer metastasis by derepressing let-7's suppression on its target HMGA2-mediated EMT. *Tumour Biol* 35:9163–9169.
7. Lee S, et al. (2016) Noncoding RNA NORAD regulates genomic stability by sequestering PUMILIO proteins. *Cell* 164:69–80.
8. Rossi MN, Antonangeli F (2014) LncRNAs: New players in apoptosis control. *Int J Cell Biol* 2014:473857.
9. Cao L, Zhang P, Li J, Wu M (2017) *LAST*, a c-Myc-inducible long noncoding RNA, cooperates with CNBP to promote *CCND1* mRNA stability in human cells. *eLife* 6:e30433.
10. Hu X, et al. (2014) A functional genomic approach identifies FAL1 as an oncogenic long noncoding RNA that associates with BMI1 and represses p21 expression in cancer. *Cancer Cell* 26:344–357.
11. Archer K, et al. (2015) Long non-coding RNAs as master regulators in cardiovascular diseases. *Int J Mol Sci* 16:23651–23667.
12. Schmitt AM, Chang HY (2016) Long noncoding RNAs in cancer pathways. *Cancer Cell* 29:452–463.
13. Prensner JR, Chinnaiyan AM (2011) The emergence of lncRNAs in cancer biology. *Cancer Discov* 1:391–407.
14. Yang SZ, et al. (2017) The long non-coding RNA HOTAIR enhances pancreatic cancer resistance to TNF-related apoptosis-inducing ligand. *J Biol Chem* 292:10390–10397.
15. Richard JLC, Eichhorn PJA (2018) Deciphering the roles of lncRNAs in breast development and disease. *Oncotarget* 9:20179–20212.
16. Hayes EL, Lewis-Wambi JS (2015) Mechanisms of endocrine resistance in breast cancer: An overview of the proposed roles of noncoding RNA. *Breast Cancer Res* 17:40.
17. Hanahan D, Weinberg RA (2011) Hallmarks of cancer: The next generation. *Cell* 144: 646–674.
18. Chen QN, Wei CC, Wang ZX, Sun M (2017) Long non-coding RNAs in anti-cancer drug resistance. *Oncotarget* 8:1925–1936.
19. Leucci E, et al. (2016) Melanoma addiction to the long non-coding RNA SAMMSON. *Nature* 531:518–522.
20. Luo G, et al. (2015) Long non-coding RNA MEG3 inhibits cell proliferation and induces apoptosis in prostate cancer. *Cell Physiol Biochem* 37:2209–2220.
21. Liu E, Liu Z, Zhou Y, Mi R, Wang D (2015) Overexpression of long non-coding RNA PVT1 in ovarian cancer cells promotes cisplatin resistance by regulating apoptotic pathways. *Int J Clin Exp Med* 8:20565–20572.
22. Ghanam AR, et al. (2017) Shining the light on senescence associated LncRNAs. *Aging Dis* 8:149–161.
23. Matallanas D, et al. (2007) RASSF1A elicits apoptosis through an MST2 pathway directing proapoptotic transcription by the p73 tumor suppressor protein. *Mol Cell* 27: 962–975.
24. Guo C, Zhang X, Pfeifer GP (2011) The tumor suppressor RASSF1A prevents dephosphorylation of the mammalian STE20-like kinases MST1 and MST2. *J Biol Chem* 286:6253–6261.
25. Jaumot M, Hancock JF (2001) Protein phosphatases 1 and 2A promote Raf-1 activation by regulating 14-3-3 interactions. *Oncogene* 20:3949–3958.
26. Kilili GK, Kyriakis JM (2010) Mammalian Ste20-like kinase (Mst2) indirectly supports Raf-1/ERK pathway activity via maintenance of protein phosphatase-2A catalytic subunit levels and consequent suppression of inhibitory Raf-1 phosphorylation. *J Biol Chem* 285:15076–15087.
27. Takahashi H, et al. (2015) Significance of polypyrimidine tract-binding protein 1 expression in colorectal cancer. *Mol Cancer Ther* 14:1705–1716.
28. Cheung HC, et al. (2009) Splicing factors PTBP1 and PTBP2 promote proliferation and migration of glioma cell lines. *Brain* 132:2277–2288.
29. Cho S, Kim JH, Back SH, Jang SK (2005) Polypyrimidine tract-binding protein enhances the internal ribosomal entry site-dependent translation of p27Kip1 mRNA and modulates transition from G1 to S phase. *Mol Cell Biol* 25:1283–1297.
30. Flores JM, Martín-Caballero J, García-Fernández RA (2014) p21 and p27 a shared senescence history. *Cell Cycle* 13:1655–1656.
31. Sears R, et al. (2000) Multiple Ras-dependent phosphorylation pathways regulate Myc protein stability. *Genes Dev* 14:2501–2514.
32. Okamoto T, et al. (2014) Enhanced stability of Mcl1, a prosurvival Bcl2 relative, blunts stress-induced apoptosis, causes male sterility, and promotes tumorigenesis. *Proc Natl Acad Sci USA* 111:261–266.
33. Huang J, et al. (2014) Long non-coding RNA UCA1 promotes breast tumor growth by suppression of p27 (Kip1). *Cell Death Dis* 5:e1008.
34. Akrami R, et al. (2013) Comprehensive analysis of long non-coding RNAs in ovarian cancer reveals global patterns and targeted DNA amplification. *PLoS One* 8:e80306.
35. Takenaka K, et al. (2016) The emerging role of long non-coding RNAs in endometrial cancer. *Cancer Genet* 209:445–455.
36. Ferrè F, Colantoni A, Helmer-Citterich M (2016) Revealing protein-lncRNA interaction. *Brief Bioinform* 17:106–116.
37. Liu PY, et al. (2014) Effects of a novel long noncoding RNA, lncUSMycN, on N-Myc expression and neuroblastoma progression. *J Natl Cancer Inst* 106:dju113.
38. Dhillon AS, Meikle S, Yazici Z, Eulitz M, Kolch W (2002) Regulation of Raf-1 activation and signalling by dephosphorylation. *EMBO J* 21:64–71.
39. Kerkhoff E, et al. (1998) Regulation of c-myc expression by Ras/Raf signalling. *Oncogene* 16:211–216.
40. Sears R, Leone G, DeGregori J, Nevins JR (1999) Ras enhances Myc protein stability. *Mol Cell* 3:169–179.
41. Tsai WB, et al. (2012) Activation of Ras/PI3K/ERK pathway induces c-Myc stabilization to upregulate argininosuccinate synthetase, leading to arginine deiminase resistance in melanoma cells. *Cancer Res* 72:2622–2633.
42. Thomas LR, Tansey WP (2011) Proteolytic control of the oncoprotein transcription factor Myc. *Adv Cancer Res* 110:77–106.
43. Escamilla-Powers JR, Sears RC (2007) A conserved pathway that controls c-Myc protein stability through opposing phosphorylation events occurs in yeast. *J Biol Chem* 282: 5432–5442.
44. Vicencio JM, et al. (2008) Senescence, apoptosis or autophagy? When a damaged cell must decide its path–A mini-review. *Gerontology* 54:92–99.
45. Biran A, et al. (2017) Quantitative identification of senescent cells in aging and disease. *Aging Cell* 16:661–671.
46. Leicht DT, et al. (2007) Raf kinases: Function, regulation and role in human cancer. *Biochim Biophys Acta* 1773:1196–1212.
47. Santarpia L, Lippman SM, El-Naggar AK (2012) Targeting the MAPK-RAS-RAF signaling pathway in cancer therapy. *Expert Opin Ther Targets* 16:103–119.
48. Rodríguez-Berriguete G, et al. (2012) MAP kinases and prostate cancer. *J Signal Transduct* 2012:169170.
49. Yang S, Liu G (2017) Targeting the Ras/Raf/MEK/ERK pathway in hepatocellular carcinoma. *Oncol Lett* 13:1041–1047.
50. Campisi J (2005) Senescent cells, tumor suppression, and organismal aging: Good citizens, bad neighbors. *Cell* 120:513–522.
51. Mooi WJ, Peeper DS (2006) Oncogene-induced cell senescence–Halting on the road to cancer. *N Engl J Med* 355:1037–1046.
52. Elmore S (2007) Apoptosis: A review of programmed cell death. *Toxicol Pathol* 35: 495–516.
53. Fulda S, Debatin KM (2006) Extrinsic versus intrinsic apoptosis pathways in anticancer chemotherapy. *Oncogene* 25:4798–4811.
54. Song H, et al. (2010) Mammalian Mst1 and Mst2 kinases play essential roles in organ size control and tumor suppression. *Proc Natl Acad Sci USA* 107:1431–1436.
55. Zhao B, Li L, Lei Q, Guan KL (2010) The Hippo-YAP pathway in organ size control and tumorigenesis: An updated version. *Genes Dev* 24:862–874.
56. Collado M, Blasco MA, Serrano M (2007) Cellular senescence in cancer and aging. *Cell* 130:223–233.
57. Hinds P, Pietruska J (2017) Senescence and tumor suppression. *F1000 Res* 6:2121.
58. Childs BG, Baker DJ, Kirkland JL, Campisi J, van Deursen JM (2014) Senescence and apoptosis: Dueling or complementary cell fates? *EMBO Rep* 15:1139–1153.
59. Michaloglou C, et al. (2005) BRAFE600-associated senescence-like cell cycle arrest of human naevi. *Nature* 436:720–724.
60. te Poele RH, Okorokov AL, Jardine L, Cummings J, Joel SP (2002) DNA damage is able to induce senescence in tumor cells in vitro and in vivo. *Cancer Res* 62:1876–1883.
61. Dimri GP (2005) What has senescence got to do with cancer? *Cancer Cell* 7:505–512.
62. Li Z, et al. (2016) Encorafenib (LGX818), a potent BRAF inhibitor, induces senescence accompanied by autophagy in BRAFV600E melanoma cells. *Cancer Lett* 370:332–344.
63. Xue W, et al. (2007) Senescence and tumour clearance is triggered by p53 restoration in murine liver carcinomas. *Nature* 445:656–660.
64. Dang CV (2012) MYC on the path to cancer. *Cell* 149:22–35.
65. Nilsson JA, Cleveland JL (2003) Myc pathways provoking cell suicide and cancer. *Oncogene* 22:9007–9021.
66. Sears RC (2004) The life cycle of C-myc: From synthesis to degradation. *Cell Cycle* 3: 1133–1137.
67. Dai MS, Sears R, Lu H (2007) Feedback regulation of c-Myc by ribosomal protein L11. *Cell Cycle* 6:2735–2741.
68. Farrell AS, Sears RC (2014) MYC degradation. *Cold Spring Harb Perspect Med* 4: a014365.
69. Posternak V, Cole MD (2016) Strategically targeting MYC in cancer. *F1000 Res* 5:408.
70. Dong L, et al. (2011) Ets-1 mediates upregulation of Mcl-1 downstream of XBP-1 in human melanoma cells upon ER stress. *Oncogene* 30:3716–3726.
71. Tuli L, Ressom HW (2009) LC-MS based detection of differential protein expression. *J Proteomics Bioinform* 2:416–438.
72. Xiang S, et al. (2018) LncRNA IDH1-AS1 links the functions of c-Myc and HIF1α via IDH1 to regulate the Warburg effect. *Proc Natl Acad Sci USA* 115:E1465–E1474.
73. Wang JY, et al. (2017) Skp2-mediated stabilization of MTH1 promotes survival of melanoma cells upon oxidative stress. *Cancer Res* 77:6226–6239.
74. Tay KH, et al. (2012) Suppression of PP2A is critical for protection of melanoma cells upon endoplasmic reticulum stress. *Cell Death Dis* 3:e337.
75. Hu WL, et al. (2018) GUARDIN is a p53-responsive long non-coding RNA that is essential for genomic stability. *Nat Cell Biol* 20:492–502.